Solid Freeform Fabrication 2023: Proceedings of the 34th Annual International Solid Freeform Fabrication Symposium – An Additive Manufacturing Conference
Reviewed Paper

3D Printing of Passive Microfluidic Flow Mixers Using Triply Period Minimal Surface Microlattice Structures

Mazher Iqbal Mohammed

School of Design and Creative Arts, Loughborough University, Loughborough, UK, LE11 3TU

Abstract

Microfluidics are miniaturised devices useful for precision fluid handling phases when conducting a range of chemical reactions or biological processes. Such devices operate at micrometre length scales, where laminar flow dominates and so interactions are limited to diffusion between the flowing liquid interfaces unless flow is made turbulent to induce mixing. Passive mixers are desirable for this task as they comprise geometrical features which can be incorporated during the fabrication of such devices. Designs largely remain planar due to traditional microfluidic manufacturing being conducted with 2.5D fabrication processes. Additive Manufacturing now allows for passive mixers to now be realised in true 3D but have seen limited investigation. This study explores the efficacy of several miniaturised Triply Period Minimal Surface micro-lattice structures, formed within microfluidic channels as turbulence inducing structures for increased mixing. We explore several lattice designs and report on their efficacy for mixing reactions conducted during continuous flow conditions.

1 Introduction

Microfluidic devices have proven a versatile tool for a range of fluidic handling processes, which have found usefulness in field ranging across chemistry, biomedical diagnostics, and environmental sampling [1,2]. Interest in microfluidics is due to the length scales of such devices, which enables them to consume low volumes of what can often be expensive/limited reagents, they can allow for multiplex reaction processes and importantly have high surface to volume ratios, resulting in fast reaction development to endpoint as compared to reactions conducted at the macro scale [3].

Historically, microfluidic devices are manufactured using processes adopted from the microelectronics industry, in particular photolithography. Manufacturing of microfluidic devices requires the use of a cleanroom and several labour intensive and time-consuming phases to create a single device. Consequently, to overcome these shortcomings a second generation of device development occurred using rapid prototyping techniques such as laser cutting/engraving [4], micro milling [5], and more recently using Additive Manufacturing (AM) processes [6]. AM technology has matured considerably over the last decade, with a growing wealth of different printing systems each capable of utilising a wide range of materials. As such microfluidic devices have been demonstrated utilising Selective Laser Melting (SLM) [7], stereolithography (SLA) [8], Fused Filament Fabrication (FFF) [9] and agarose extrusion printing to form hydrogel channels [10]. Of all these processes SLA AM holds considerable

potential for microfluidic applications, owing to the availability of transparent material variants, which allow for easy visualisation of chemical/biological processes, prints have low surface roughness, and fabrication can potentially achieve length scales of the order of one to hundreds of microns. As such there is growing interest in SLA for microfluidic applications.

The length scales of microfluidic systems cause laminar flow for most flow regimes [11]. The consequence of this is that migrating fluids remain in confined flow streams with very little mixing occurring outside of modest diffusion at the flowing fluid boundaries. To resolve this issue, the use of active or passive mixers can disrupt laminar flow by inducing inertial forces within the bulk of the flowing fluid [12]. While both are effective means of mixing, passive structures are desirable as they require no moving components, reducing design and fabrication complexity and can be manufactured using the same fabrication processes used to form the microfluidic channel structures [13]. Historically, passive mixing structures have generally been designed to be planar in geometry, largely based on the design constraints of the typically employed 2.5D manufacturing processes (e.g. photolithography, laser engraving, etc). With the new generation of AM fabricated microfluidic systems, there is now the potential to realise mixing structures which are designed in true 3D within fluidic channels, generating new modes of turbulence. Lattice structures would be ideal candidates for such applications, as they comprise complex geometrical configurations with porosity, which would allow for free migration of a fluid through the bulk of the structure. Of the wide number of possible lattice configurations, Triply Period Minimal Surface (TPMS) geometries have been gathering considerable interest owing to their complex symmetries [14] and geometry which does not require the use of support structures [15]. Recent studies have also begun to explore the uses of TPMS and wider micro-lattice structures in applications for impact absorption [16] and acoustic dampening [17], however none have explored uses in microfluidic applications.

In this study we present preliminary work regarding the fabrication and experimental examination of TPMS lattice structures manufactured in situ within microfluidic channels, with the purpose of inducing mixing of two migrating fluids which otherwise would experience laminar flow. We believe this to be the first study which has made use of lattice structure for such an application. As microfluidic devices are systems which geometrically are at micro length scales, we focus on the manufacturability of such systems using SLA fabrication processes, exploring smallest attainable channel size, alongside fabrication dimensional accuracy. We then demonstrate the capability of creating repeatable microchannels containing lattice structures, alongside a simple and novel lamination fabrication method to seal the devices for use. We also present a universal luer lock design which complements the intended fluidic flow-based application, before assessing the mixing within such structures. Surprisingly, it was found that laminar flow can occur through the bulk of the lattice structure despite the geometrical barriers inducing inertial forces within the flow, and therefore turbulence. However, we demonstrate that through an interplay of lattice size, unit cell type and flow rate of the migrating fluid, we can generate turbulent flow and mixing of two, coloured dye solutions migrating through the lattice structure. We present our initial findings and hope this to be a catalyst for further inquiry.

2 Methods

2.1 Microfluidics design

Microfluidic networks were designed using a combination of Fusion 360 (Autodesk, UK) and nTopology 3.44.4 (nTopology, USA) CAD software. The overall design of a fluid device comprised a double laminate layer. The lower layers were designed using nToplogy and comprised a standard t-channel mixing system, with entry channels 5mm long and a mixing channel which was 30mm long. The various lattice structures were designed to be the height of the channel and placed 2mm into the straight mixing channel of the t-chip. Lattice structures were formed from various Gyroid and Diamond TPMS unit cells. Fusion 360 was used to form the top layer of each device, which seals the channel and has ports for fluidic entry. For testing purposes, microfluidic channels were kept to a fixed cross section, comprising a height and width of 1mm. The TPMS structures were trialled with varying unit cell sizes of 0.3 to 1mm, which are within the acceptable size range for the proposed channels. For fabrication tests, a unit cell of a given size was projected through a rectangular structure, with a cross section of 1x1 and length 30mm. For fluidic testing a given unit cell was projected through a 5mm long rectangle with a cross section of 1x1mm.

2.2 Microfluidic manufacturing

From preliminary in-house testing (results not shown) it was found that direct AM of closed microfluidic devices with the TPMS structures containing within a channel resulted in blockages which impeded fluid flow until relatively large design geometries (approximately >3mm features). This was in part due to the enclosed area impeding resin removal within the channel and lattice during fabrication, and consequently resulting in partial curing within the channel/lattice structures. By contrast, printing the microchannel and microlattice structures as open, unsealed structures allowed for uncured resin to migrate out of channel and lattice structures due to gravity, resulting in superior design reproduction. Owing to the improved fabrication reproduction, open structures were considered the preferred approach in this study, however necessitated post sealing of the fluidic chip through lamination.

The lower laminate layer containing the lattice and microfluidic channels structures were manufactured using a Direct Light Projection (DLP) based vat polymerisation 3D printing process using a commercially available desktop printing system (LD006, Creality, China). This system operated such that the printing build platform is inverted and the raises and lowers into a vat of photocurable polymer, which contains a clear window at the bottom for the projection of ultraviolet light from a TFT screen. The final devices are fabricated by the build platform submerging within the resin to a set distance (layer height) from the TFT screen, where the pattern of the microchip layer is projected into the vat by selective lighting of the TFT screens pixels, resulting in polymerisation of the resin onto the build surface. This process is then repeated layer by layer until the complete chip has been fabricated. The system has a manufacturer stated resolution of 0.05mm in the XY and 0.01mm in the Z. All microfluidic chips were manufactured using a commercially available clear acrylate-based photopolymer (Clear Hard Resin, Technology Outlet, UK). Slicing of a given design and generation of machine printing instructions was achieved using Chitubox open-source software (v1.9.4,

Chitbubox, China), using a fixed layer height of 30µm, a bottom layer count of 10, layer exposure time of 2s and bottom layer exposure time of 15s.

Once a respective microfluidic chip had been fabricated and removed from the printer, it was placed into an agitating cleaning bath (Form Wash, Formlabs, USA) filled with a resin cleaning solution (Resin Cleaner 30, Photocentric, UK) and washed for 15 minutes. Following cleaning, excess residual solution was removed using compressed air, before the device was placed into a UV curing chamber for 30 minutes to allow for the complete curing of resin within the bulk of the device. Following exposure devices were ready for bonding of the upper laminate layer.

The upper laminate layers were fabricated in 2mm thickness acrylic sheets using a commercial CO_2 laser cutter (X252, GCC LaserPro, UK). Prior to laser cutting, the acrylic was prepared with double sided tape (3M, UK) without removing the tape cover on the non-contact side and cutting was performed through both the tape and acrylic. The final laminate layers were formed by removal of the tape cover and manually aligning and firmly pressing the cover layer to the microfluidic layer, creating a sealed microfluidic chip. Acrylic was used, as its transparency allowed for clear visualisation within the fluidic chips. To interface the devices with a syringe pump, a universal luer lock entry port structure was designed, and 3D printed in the same clear resin material and adhesive bonded to the opening of the microfluidic chips.

2.3 Fluidic flow and imaging

Fluidic flow in the microfluidic devices was achieved by infusion into the chip using two syringe pumps (NE-1002X, New Era, USA), which allowed for flow rate adjustment from 1µl/min to 600µl/min. To visualise flow, various food dye solutions were used, which allowed sufficient contrast of the flowing fluid front and also for mixing to be assessed based on the proportion of new colour formation from the two input colours. Flow and mixing of fluids on chip were imaged using a USB microscope camera (AM4917MZT, Dinolite, Taiwan).

3 Results

3.1 Print Fabrication Resolution Tests

Microfluidic devices are typically at length scales from a single to hundreds of micrometres, which makes their fabrication often quite challenging. For many AM technologies this would mean fabrication near the limits of build resolution. As such it is important to appreciate the typical length scales which are achievable for both fabrication of the microfluidic channels and the internal lattice structures, with lattice features likely to be an order of magnitude smaller. To assess the attainable build resolution, tests were initially conducted to determine the lower build limits with the given 3D printer and resin combination. This was achieved through the design of a test structure, which included various rectangular channel and raised structures, and which can be seen in figures 1 and 2. In creating these test structures, we were also able to determine any discrepancies between the CAD and fabricated structures. Figure 1 shows graphs of the width and height of the constructed channel for 5 repeated measurements of the channel cross sectional geometry, including ±1 standard deviation error.

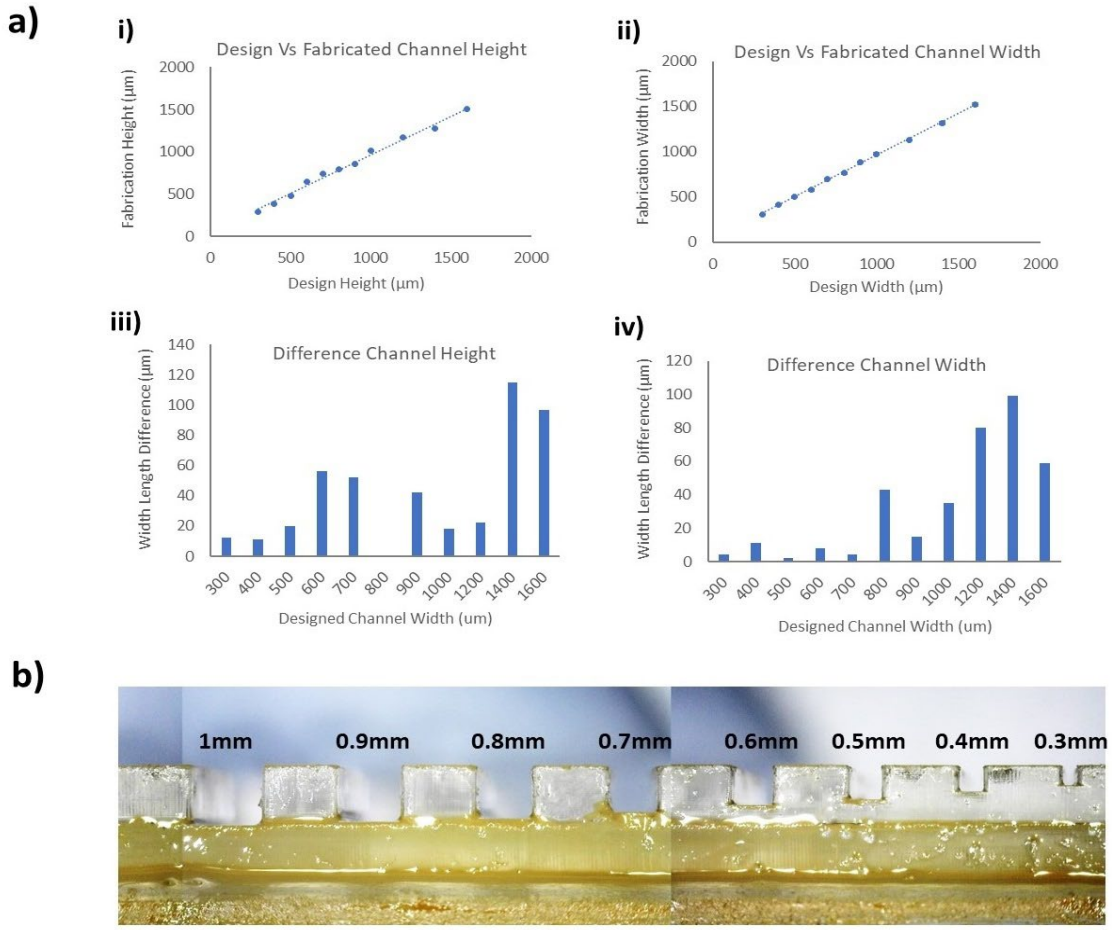

Figure 1: a) Graphs comparing the fabricated Vs designed i) height and ii) width of the channels, alongside bar graphs illustrating the difference between designed and fabricated iii) width and iv) height. b) A microscope image composite of the fabricated channel cross sections.

To assess the difference in the horizonal and vertical print resolutions, channels were designed to be of an equal width and height. It was found that the 3D printer system could repeatably produce channels down to a cross sectional area of 0.3x0.3mm. However, it was found that the resulting channels could often be partially blocked meaning while the resolution was attainable it was not repeatable for the given settings. We therefore concluded a channel cross section of 0.4x0.4mm to be the lower limit of channel fabrication. It was also found that the fabricated widths and heights were consistently smaller than the design geometry, with differences ranging from 0.4 to 7.1% in width and 1.8 to 8.2% in height as compared to the design geometry. We believe this is due to the inherent shrinkage of the polymer which occurs during the photo polymerisation phases of fabrication, and which has been reported in previous studies [18]. It is also noted that the smallest attainable print feature size is considerably larger than the print resolution of the printer. This is believed to be due to the relative concentration of the photoinitiator within the resin, which has been found previously to impact crosslinking density, and therefore print feature size [19]. Interestingly, in microfluidic research, it is often desirable to obtain the smallest resolution of channel structure possible due to the reduced

reagent consumption and increased reaction mixing dynamics. However, this reduction in size is marginal, measured in this study as between 4-11µm, and which reduced as the geometry approach the limits of print resolution. It was also found that the difference between designed and measured channel width/height began to increase as the length scales became larger, increasing the difference up to 115µm at geometries >1.4mm. This again would be expected due to the cumulative shrinking effect over many more layers at these geometries. Figure 1b) shows images of the fabricated channel cross sections, where it can be seen there is reasonable geometrical accuracy, resulting in well-defined square cross sections. It is noted that at the bottom of the channels, at the intersection of the horizontal base and vertical side walls, that the fabricated geometry becomes more curved which we believe is due to surface tension effects of the resin during photopolymerisation.

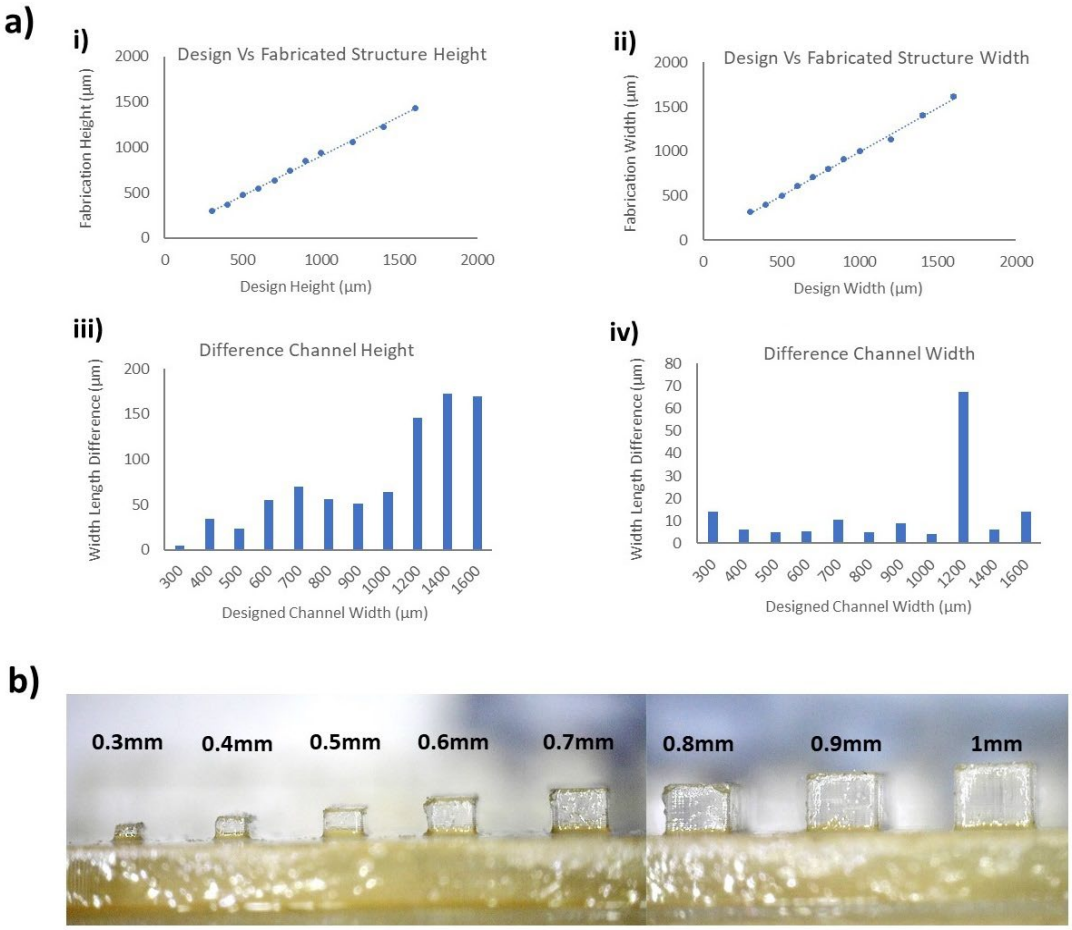

Figure 2: a) Graphs comparing the fabricated Vs designed i) height and ii) width of the raised square structures, alongside bar graphs illustrating the difference between designed and fabricated iii) width and iv) height. b) A microscope image composite of the fabricated raised square structure cross sections.

A second set of fabrication tests with a raised rectangular structure was conducted to assess the print resolution when fabricating the solid lattice structures within the channels. Figure 2 shows graphs illustrating the width and height of the constructed raised features for

five repeat measurements of the structure cross sectional geometry. The graphs including errors of ±1 standard deviation.

Comparing the results for the channel fabrication it was found that there was greater reproducibility for the width geometry, with all but the structure made at a width of 1.2mm showing deviation of >10µm between designed and fabricated structures. The higher deviation between design and fabricated structure for a width of 1.2mm was consistent between repeat tests and it is unclear why this was occurring. Ultimately, this geometry was larger than that which we would be utilising for the fabrication of the lattice structures as so the phenomenon was not investigated further. Examining the height of the raised structures, it was found there was significantly higher variability between design and fabrication heights, which reached a maximum of up to a 12.3% reduction. As with the channel fabrication tests this reduction in height can be explained in part due to shrinkage, however the higher percentage would imply a greater shrinkage. Another possible explanation could be due to the nature of the printing process given fabrication occurs with structures on the build platform being raised and lowered into the vat. During this time either surface tension effects between the part and the exposure area or minoring shearing of uncured surface material could explain the reduced height. It is noted that in figure 2b) several of the imaged structures have a distorted upper region to the square structure, which would be consistent with either damage or non-uniform curing. This would therefore support the argument that the height differences are due to shearing or surface tension effects, we hope to examine the cause of this issue in future work.

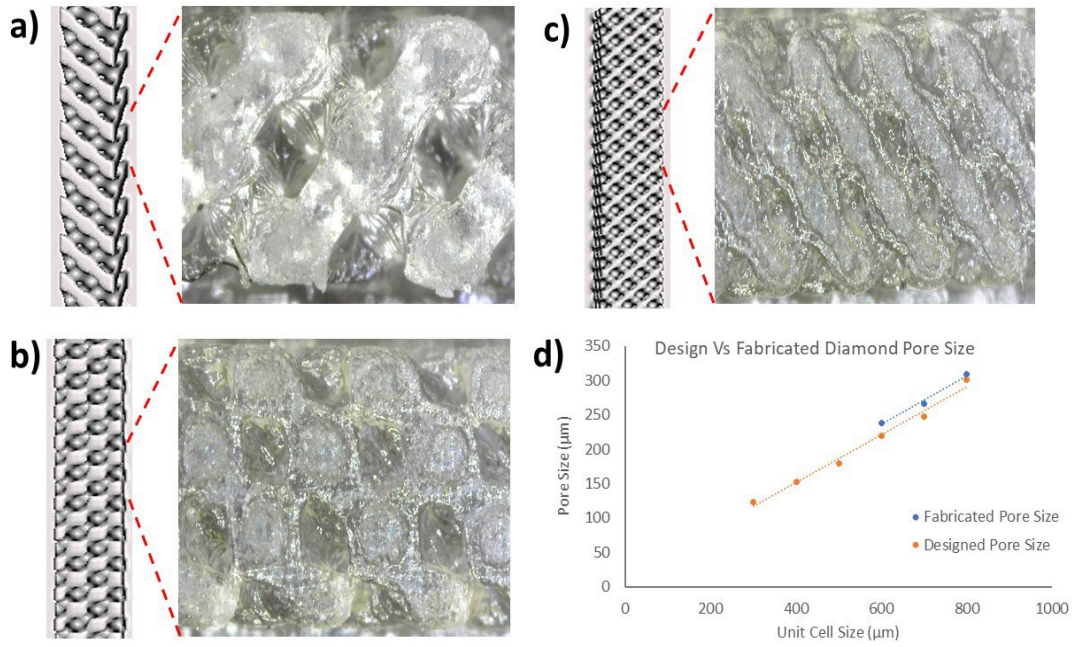

Figure 3: Microscope images of the fabricated micro-lattice structures for a Diamond unit cell size of a) 0.8mm, b) 0.6mm and c) 0.4mm. d) a Graph illustrated the designed and fabricated micro-lattice structures for unit cell size against the resulting pore size. Note: fabrication data only includes for 0.8, 0.7 and 0.6mm unit cell sizes, as below these geometries the lattice structures were found to be closed.

3.2 Micro-lattice Fabrication Tests

The proposed lattice structures in this study are to be printed at micro scale geometries, which would be at the limit of resolution of the printer. To therefore verify the smallest attainable lattice structures and their structural repeatability several fabrication tests were conducted to determine a suitable geometry for flow mixing tests. Figure 3 illustrates the fabrication tests for a Diamond TPMS structure which was designed and fabricated using unit cell sizes of 0.3, 0.4, 0.5, 0.6, 0.7 and 0.8mm. It was found that for unit cell sizes of ≤0.5mm fabricated structures would have closed pores within the scaffold and so the fabrication limit was determined to be a minimum unit cell size of 0.6mm. As it can be seen in the graph in figure 3d), the fabricated pore size was marginally larger than the designed pore size by approximately 8-19µm. It is not entirely clear why the fabricated geometry would be larger than the design geometry given shrinkage effects. This may be related to surface tension effects of the resin within the Diamond lattice structure during fabrication or could be due to marginal over exposure of the structure given the spatial geometry. Further adjustments to the exposure were not explored but will be the subject of future work. The limits of design for fabrication revealed a lower pore size of 238±3.6µm, which can be assumed to be the fluidic channel geometry when a fluidic would migrate through such a lattice. Interestingly, this geometry is approximately twice as small as the smallest, repeatably fabricated microfluidic channel.

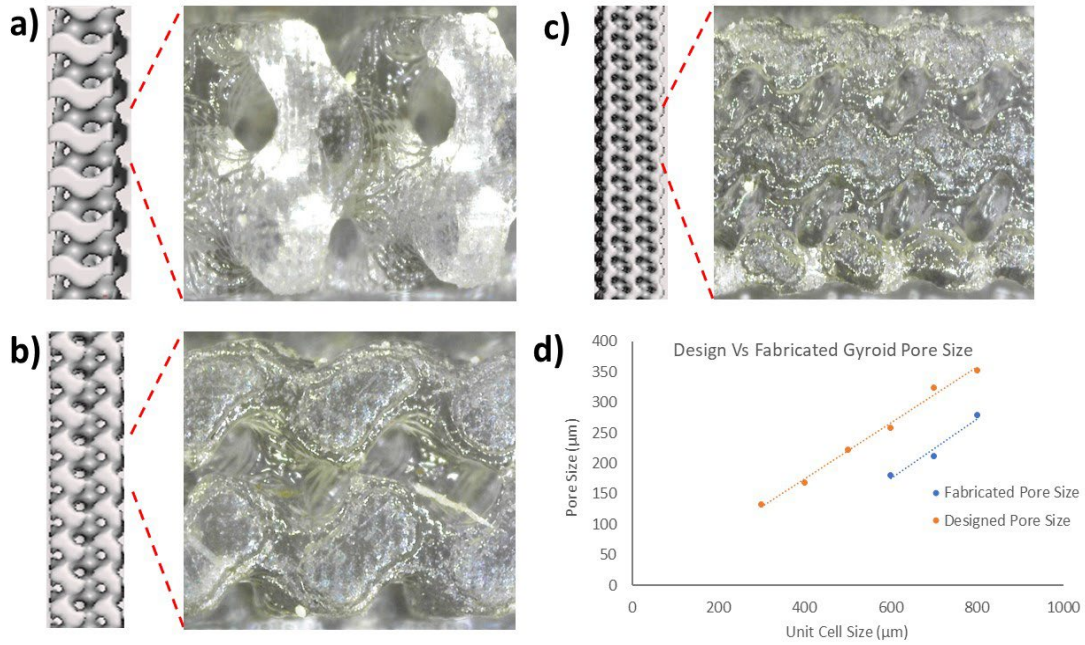

Figure 4: Microscope images of the fabricated micro-lattice structures for a Gyroid unit cell size of a) 0.8mm, b) 0.6mm and c) 0.4mm. d) a Graph illustrated the designed and fabricated micro-lattice structures for unit cell size against the resulting pore size. Note: fabrication data only includes for 0.8, 0.7 and 0.6mm unit cell sizes, as below these geometries the lattice structures were found to be closed.

Figure 4 illustrates the fabrication tests for various Gyroid TPMS structures which were again designed and fabricated using unit cell sizes of 0.3, 0.4, 0.5, 0.6, 0.7 and 0.8mm. As with

the diamond structures, it was found that for unit cell sizes of ≤0.5mm, fabricated structures would have closed pores within the scaffold and so the fabrication limit was determined to be a minimum unit cell size of 0.6mm. Examining the graph in figure 4d, the fabricated pore size was lower than the designed pore size by approximately 74-111µm, which amounted to a 20-34% reduction in size compared to the design. The reduction in size between the fabricated and designed pores are consistent with the previous results which showed a shrinkage in the material. However, on this occasion shrinkage is significantly larger than that found during the channel and raised structure tests. Based on our finding we believe this to be geometry related given the differences between Gyroid and Diamond designs, and how these influence the resin residency within the structures due to surface tension effects of the resin within the lattice pores. We hope to further investigate material shrinkage in future work. The limits of design for fabrication revealed a lower pore size of 180±4.2µm, which again can be assumed to be the fluidic channel geometry when a fluidic would migrate through such a lattice.

3.3 Fluidic Mixing tests

Following confirmation of design for fabrication limits within the SLA system, a trial geometry comprising channel cross section of 1x1mm was selected for flow testing. Given that the minimum cell size was found to be 600µm, a test TPMS lattice unit cell of 1mm was tested to understand the mixing potential of the micro-lattice.

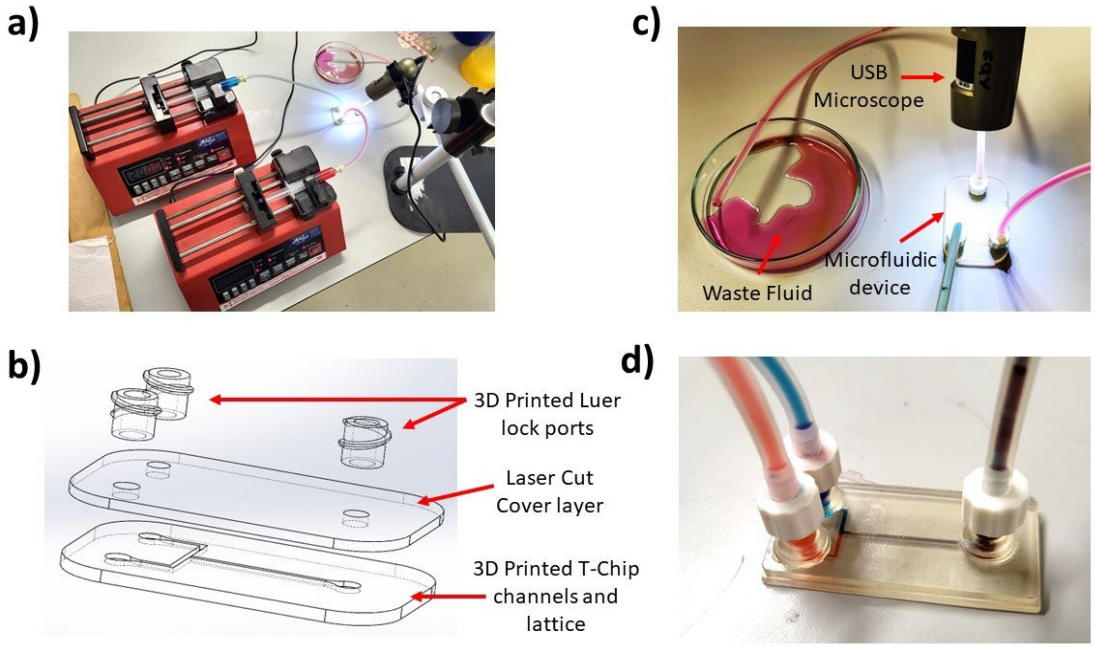

Figure 5: a) The experimental set-up for flow testing, comprising two syringe pumps, various silicone tubing and Luer locks to interface with the microfluidic device and a USB microscope to visualise flow. b) A diagram illustrating the laminate layer design of the fluidic chips, alongside the 3D Printed Luer lock adaptors. c) A close-up view of the fluidic chip and d) An example of a fluidic chip containing a Diamond lattice structure, where mixing of the red and blue inputs results in purple at the output.

Figure 5 illustrates the experimental set up for the flow tests, along with an example of a final microfluidic chip fabricated using laminate hybrid manufacturing, combining 3D printing and laser cutting processes. Initially, a t-chip containing no lattice structures was fabricated to test the flow dynamics, where it was found that laminar flow was observed across the examined flow rates between 1µl/min and 600µl/min (results not shown). Given the geometry of the microfluidic channels, a minimum flow rate of 20µl/min was utilised such that flow dynamics would reach a steady state over the course of minutes, allowing for a rapid assessment of changes in flow kinematics. The flow rate was also kept the same for both flow streams to ensure there was an even volume of each food dye during interactions.

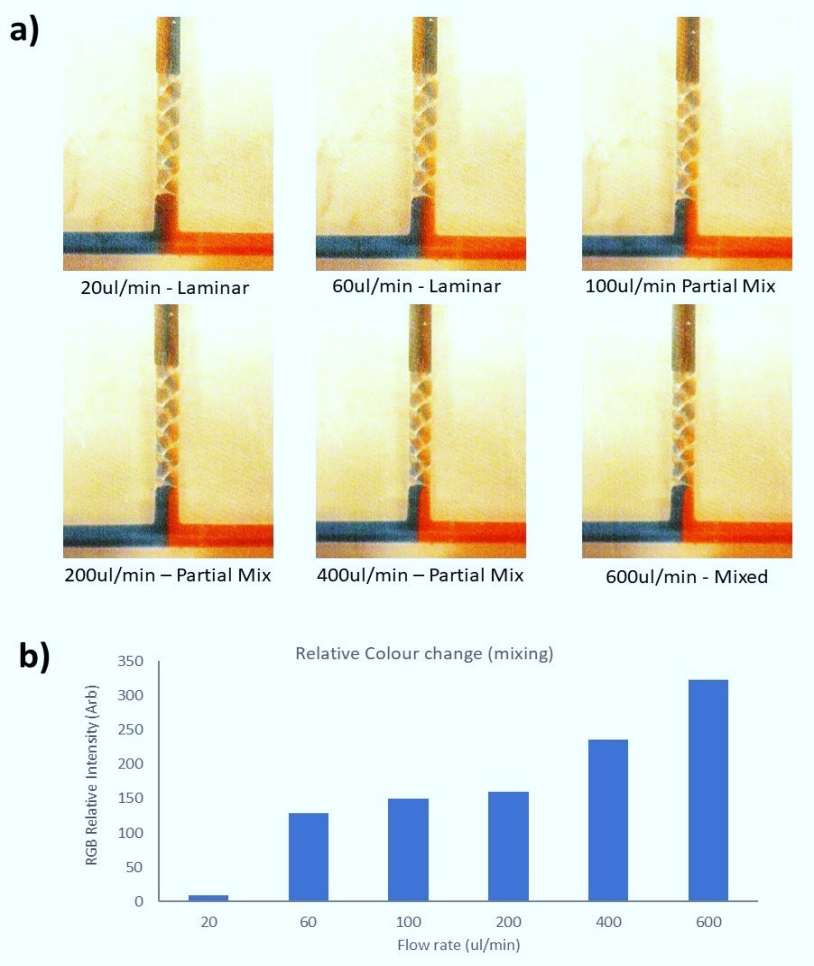

Figure 6: a) Images of the steady state flow within the micro-lattice containing microfluidic devices for changes in the flow rate of the input flow channels. b) A graph illustrating the change in the colour at the output of the microfluidic channel, with greater depth of colour change signifying increased mixing.

Figure 6a shows the steady state flow streams for various flow rates within a t-chip containing a 5mm length of Diamond micro-scaffold. It was observed that there was disruption of laminar flow for flow rates >60µl/min. Mixing occurs primarily due to either diffusion within the bulk of a fluid, or due to inertial forces within a microfluidic system, as diffusion is limited in

laminar flow, all mixing is likely occurring due to inertial effects. It is therefore believed that the inertial forces due to the directional changes in the micro-lattice are responsible for mixing. Interestingly, it was found that the flow channels switched sides within the single channel from the input flow streams, as can be seen for the 20µl/min flow tests. Typically, this would not be observed in such systems. The migration of the fluids to opposite sides of the microfluidic channel may imply that the two flow streams effectively take a zig zag path as they migrate through the micro-lattice and which has a small radius of curvature, thereby not generating substantial inertial forces and mixing. Additionally, the number of repeating unit cells within a length of micro-lattice may also influence the migration. In these tests there were five complete unit cells in the lattice, and so the odd number of cells may cause the migration. To test this assumption a second system was created with a two unit cell containing micro-scaffold and indeed the flow was found to remain unperturbed (results not shown). We believe this to be the first report of geometrical changes within a channel structure allowing for migration of laminar flow paths to new regions of a microfluidic channel.

Another interesting observed phenomenon was the preservation of partial flow streams, which were observed at flow rates of ≥200ul/min, which is visible in figure 6a) as the small blue flow stream at the centre of the channel. The dynamics of how this is occurring is less understood but will be the subject of future studies. Ultimately, it was demonstrated that the micro-lattice structure provides a passive means of generating turbulent flow within a 3D printed microfluidic system, albeit within a specific range of flow rates.

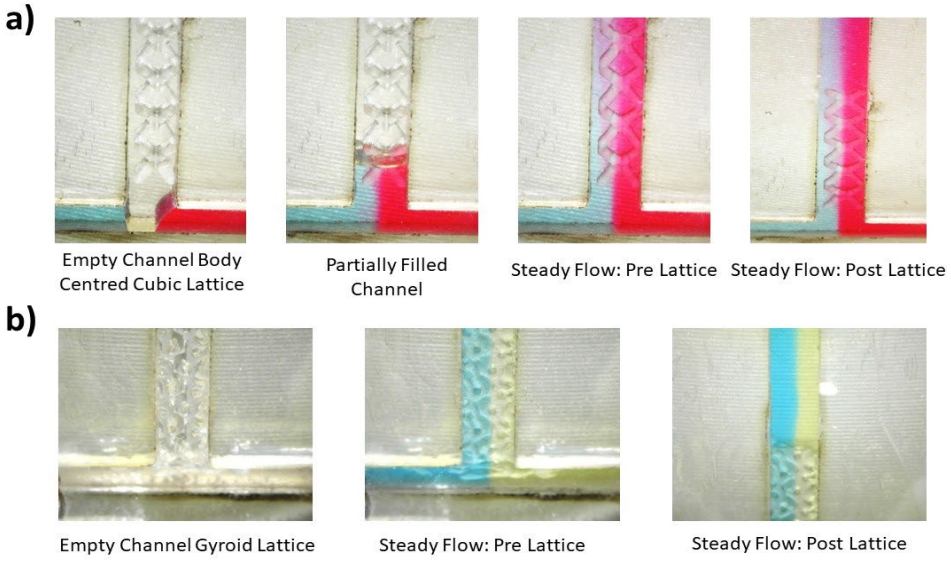

Figure 7: Time lapsed images of fluid entering a t-chip containing a) a body centred cubic lattice structure and b) a Gyroid structure.

3.4 Laminar Flow within Micro Lattice

During the study, an unexpected phenomenon was discovered within the micro-lattice structures, namely that for certain configurations laminar flow was found to continue through the bulk of the lattice and beyond the lattice boundary. Figure 7 illustrates two configurations of lattice structure which exhibited laminar flow through the bulk of the structure, with the unit

cells comprising a Gyroid and body centred cubic geometries. Laminar flow within the lattice structures was observed at all previously tested flow rates, which was again surprising to observe. The reason for why laminar flow is occurring is uncertain, as the lattice was expected to act as an effective barrier to the directional flow of the fluid, resulting in inertial effects and ultimately mixing, however this is not what is occurring. One possible reason for the laminar flow could be that the bulk flow in the direction of the channel is larger than that which would undergo inertial effects through direction changes of the fluid, resulting in effective viscous drag force acting on the deflected fluids, driving them back into laminar flow. We hope to investigate this assertion in future work.

4 Conclusion

This study successfully demonstrates the potential of TPMS micro-lattice structures as passive mixers to disrupt laminar flow within AM fabricated microfluidic channels. We primarily show that for Diamond unit cells mixing and a range of different flow phenomena are possible. Firstly, it was found that the micro-lattice structure can move the occupancy of a flowing fluidic within a channel at lower flow rates (<200µl/min), resulting in the red and blue dye solution laminar flow streams moving from left to right respectively. This was believed to be due to the preferred fluidic flow path within the micro-lattice being an effective zigzag through the structure with a low radius of curvature for flow directional changes. These low radii of curvature of the pore flow path results in low inertial forces allowing for flow to remain laminar. Secondly, at a critical flow rate (>200ul/min), sufficient inertial forces are generated for fluids migrating through the examined Diamond micro-lattice geometry resulting in mixing. However, for the body centred cubic and Gyroid micro-lattices it was found that laminar flow occurring through the bulk of specific micro-lattice across all tested flow rates. This result was surprising, and the nature of this phenomenon is geometrically driven, implying certain unit cells may not be suitable for mixing of fluids using this approach. Thirdly, the pores produced in the smallest fabricated lattice structures allowed for the creation of fluidic channels which were approximately half the cross section of the smallest attainable microfluidic channel (approximately 180µm). Beyond microfluidic systems, lattice mediated fluidic exchange is becoming increasing popular for additively manufactured heat exchange products which would be susceptible to laminar flow, thereby limiting heat exchange capacity. Therefore, these findings may help inform suitable unit cell use and wider heat exchanger designs. It is ultimately hoped that these preliminary findings may help advance investigation of fluidic based exchange in a wider range of lattice structures.

References

[1] Soumyabrata, B., Uchil, A., Kalsang, T., Chakrabarty, S., Ali, M. A., Srisungsitthisunti, P., Mahato, K. K., Surdo, S., and Mazumder, N. -The revolution of PDMS microfluidics in cellular biology - *Critical Reviews in Biotechnology*, 1-19, 2022.

[2] Mohammed, M. I. and Desmulliez, M. P. Y. - Autonomous capillary microfluidic system with embedded optics for improved troponin I cardiac biomarker detection - *Biosensors and Bioelectronics,* vol. 61, pp. 478-484, 2014.

[3] Mohammed, M. I., Haswell, S. and Gibson I. - Lab-on-a-chip or Chip-in-a-lab: Challenges of Commercialization Lost in Translation - *Procedia Technology,* vol. 20, pp. 54-59, 2015.

[4] Mohammed, M. I., & Desmulliez, M. P. Y. (2013). The manufacturing of packaged capillary action microfluidic systems by means of CO 2 laser processing. *Microsystem technologies*, *19*, 809-818.

[5] Guckenberger, D. J., De Groot, T. E., Wan, A. M., Beebe, D. J., & Young, E. W. - Micromilling: a method for ultra-rapid prototyping of plastic microfluidic devices - *Lab on a Chip*, *15*(11), 2364-2378, 2015.

[6] Au, A. K., Huynh, W., Horowitz, L. F., & Folch, A. - 3D-printed microfluidics - *Angewandte Chemie International Edition*, *55*(12), 3862-3881, 2016.

[7] S. Sandron et al., "3D printed metal columns for capillary liquid chromatography," Analyst, 10.1039/C4AN01476F vol. 139, no. 24, pp. 6343-6347, 2014.

[8] Yafia, M., Ymbern, O., Olanrewaju, A.O., Parandakh, A., Sohrabi Kashani, A., Renault, J., Jin, Z., Kim, G., Ng, A. and Juncker, D. - Microfluidic chain reaction of structurally programmed capillary flow events - Nature, 605(7910), pp.464-469, 2022.

[9] Quero, R.F., da Silveira, G.D., da Silva, J.A.F. and de Jesus, D.P. - Understanding and improving FDM 3D printing to fabricate high-resolution and optically transparent microfluidic devices - *Lab on a Chip*, *21*(19), pp.3715-3729, 2021.

[10] Bertassoni, L.E., Cecconi, M., Manoharan, V., Nikkhah, M., Hjortnaes, J., Cristino, A.L., Barabaschi, G., Demarchi, D., Dokmeci, M.R., Yang, Y. and Khademhosseini, A. - Hydrogel bioprinted microchannel networks for vascularization of tissue engineering constructs - *Lab on a Chip*, *14*(13), pp.2202-2211, 2014.

[11] Demello, A.J. - Control and detection of chemical reactions in microfluidic systems - *Nature*, *442* (7101), pp.394-402, 2006.

[12] Lee, C. Y., Chang, C. L., Wang, Y. N., & Fu, L. M. - Microfluidic mixing: a review - International journal of molecular sciences, 12(5), 3263-3287, 2011.

[13] Lee, C. Y., Wang, W. T., Liu, C. C., & Fu, L. M. - Passive mixers in microfluidic systems: A review - *Chemical Engineering Journal*, *288*, 146-160, 2016.

[14] Mohammed, M.I. and Gibson, I. - Design of three-dimensional, triply periodic unit cell scaffold structures for additive manufacturing - *Journal of Mechanical Design*, *140* (7), 2018.

[15] Claybrook, F., Mohammed, M. and Southee, D. - Investigation of additive manufactured Split P TPMS elastomeric structures for diabetic foot insoles - *Transactions on Additive Manufacturing Meets Medicine*, *4*(1), pp.664-664, 2022.

[16] Guo, Z., Yang, R., Liu, J., Armstrong, J., Zhao, R. and Zhou, C. - Continuous Stereolithography 3D Printing of Multi-Network Hydrogels in Triply Periodic Minimal Structures (TPMS) With Tunable Mechanical Strength for Energy Absorption - ASME

International Mechanical Engineering Congress and Exposition (Vol. 86656, p. V003T03A021). American Society of Mechanical Engineers, 2022.

[17] Li, Z., Li, X., Chua, J.W., Lim, C.H., Yu, X., Wang, Z. and Zhai, W. - Architected lightweight, sound-absorbing, and mechanically efficient microlattice metamaterials by digital light processing 3D printing - Virtual and Physical Prototyping, 18(1), p.e2166851, 2023.

[18] Ling, L., Taremi, N. and Malyala, R. - A novel low-shrinkage resin for 3D printing - *Journal of Dentistry*, *118*, p.103957, 2022.

[19] Alonso, R. C. B., Brandt, W. C., Souza-Junior, E. J. C., Puppin-Rontani, R. M., & Sinhoreti, M. A. C. - Photoinitiator concentration and modulated photoactivation: influence on polymerization characteristics of experimental composites – Applied Adhesion Science 2 (1), 1-11, 2014.